Progress In Electromagnetics Research B, Vol. 48, 313–327, 2013

EXPERIMENTAL STUDY OF THE BEHAVIOR OF AN EBG-BASED PATCH ANTENNA SUBJECTED TO MECHANICAL DEFORMATIONS

Xiaoke Han, Nicolas Adnet, Isabelle Bruant, Frederic Pablo, Habiba Hafdallah Ouslimani*, Laurent Proslier, and Alain C. Priou

Energetic Mechanics Electromagnetic Laboratory, University Paris Ouest Nanterre la Défense, LEME-EA 4416, 50 rue de SÈVRES, Ville d'Avray 92410, France

Abstract—This work deals with the behavior of a patch antenna equipped with squared electromagnetic bandgap (EBG) structures and subjected to various mechanical deformations (twisting and bending deformations). The EBG structures have a stop band frequency (rejection) feature, allowing the coupling and the undesired electromagnetic interferences to be reduced. The influences of the deformations on the mutual coupling and radiation patterns of an antenna equipped of those EBG elements are experimentally studied.

1. INTRODUCTION

Telecommunication and avionic needs are increasing, and as a consequence, the number of antennas structures keeps growing on aircrafts. Most of the time, these antennas are prominent objects and lead up to manifold drawbacks such as: aerodynamic penalization, local weakening of the supporting region by the fixing holes of the antenna, prevalent structural health control and servicing, electromagnetic compatibility rules, etc. Patch antennas are excellent candidates to avoid these problems: they are thin, have a low profile and are conformable to planar and warped surfaces. Moreover, such a solution should allow the design of multifunctional antennas, achieved by gathering numerous functions embedded on the same substrate. In this kind of new multi-frequencies antennas, some

Received 22 November 2012, Accepted 28 January 2013, Scheduled 30 January 2013

* Corresponding author: Habiba Hafdallah Ouslimani (habiba.ouslimani@u-paris10.fr).

radiating elements might be close to each other, and an unwanted coupling effects might arise if there is not a suitable distance separating two successive radiating elements. These undesired coupling can be reduced using metamaterial (MTM) structures, such as EBG structures [1–6] and/or planar MTM surfaces such as Complementary Split Ring Resonator (CSRR) structures [7–9]. Commonly, this kind of EBG (electromagnetic bandgap) structures is used for planar antennal structures but is not optimally designed when deformed due to mechanical loads (except the theoretically study of [4]).

In this paper, the behavior of a patch antenna integrating EBG structures, subjected to prescribed mechanical deformations is studied. This work is a part of the MSIE[†] project, launched in October 2008 by the competitiveness French ASTech cluster and closed in December 2011. In Sections 2 and 3, the experimental setup and design of the EBG-based patch antenna are described. In Section 4, the experimental results are presented in planar and distorted configurations. They show that the twisting and bending loads do not affect the performance of the EBG-based patch antenna.

2. EXPERIMENTAL SETUP

Due to increasing needs in navigation, communication and surveillance, aircrafts are equipped with more and more antennal structures. Then, the antenna radiating elements have to be closer from each other and thus, reducing their mutual coupling arises from such a design constraint. A solution can consist in using metamaterial structures to reduce electromagnetic interactions between the antenna radiating elements, such as EBG structures [1–6], Complementary Split Ring Resonator (CSRR) structures [7, 9] and/or the planar MTM surfaces [8].

In flight conditions, planes are subjected to aerodynamic loads leading to the structure distortion. Flight cycles induce a combination of twist and bend modes to wings. In order to study the impact of this kind of modes on the electromagnetic behavior of EBG-based patch antenna, an experimental setup has been conceived. Fig. 1 presents this developed benchmark experimental setup [10]. It allows twisted and bended mechanical deformations of the MTM antenna in flight range defined by the aeronautical project partners. The mechanical system is composed of two main parts: part A sets a twisted configuration (Fig. 1(b)), and part B (Fig. 1(c)) is dedicated to reaching the aimed bent state.

[†] MSIE (Matériaux et Structures Intelligences pour l'Éectromagnétisme/Smart Material and Structures for Electromagnetism).

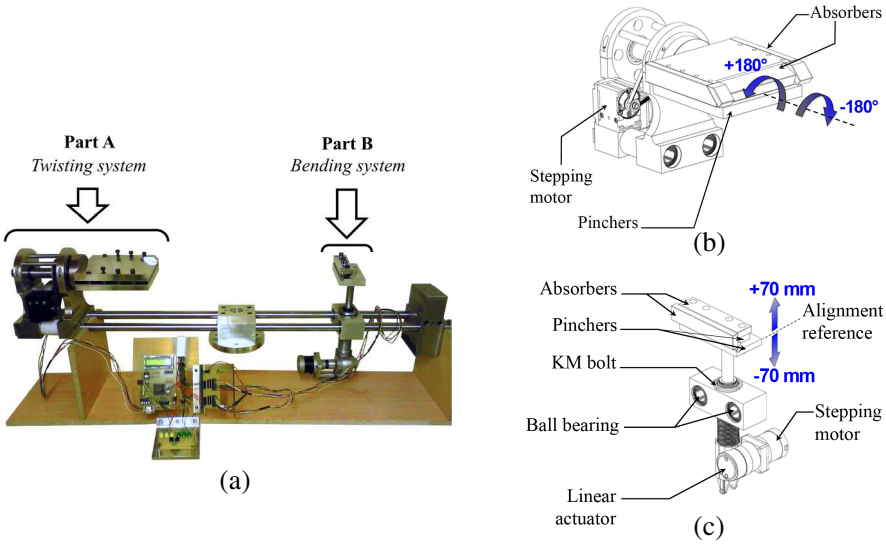

Figure 1. Experimental set up, (a) general view, (b) twisting system and (c) bending system.

The bending magnitude varies from −70 mm to 70 mm, and the twist angle covers the whole angular range from −30 to 30 degrees. The experimental set up allows the study of samples of 1 m maximum length.

When integrated with an electromagnetic measurement system (in an anechoic chamber), this set up is able to provide the antenna radiation characteristics under the considered mechanical deformations.

3. DESIGN OF THE ANTENNA AND EBG STRUCTURES

3.1. EBG Structure Features

The metamaterial EBG array structure, designed using CST MWS [11], is presented in Fig. 2(a). It consists of four EBG squared patches of 8.4 mm side length (w), spaced by a 0.275 mm gap (g) and fed by a cylindrical via of 0.5 mm diameter (d). This array structure is printed on a 0.787 mm height substrate with a permittivity equal to 2.25.

The EBG is characterized by the surface wave propagation measurement, using the setup presented Fig. 2(b), where two

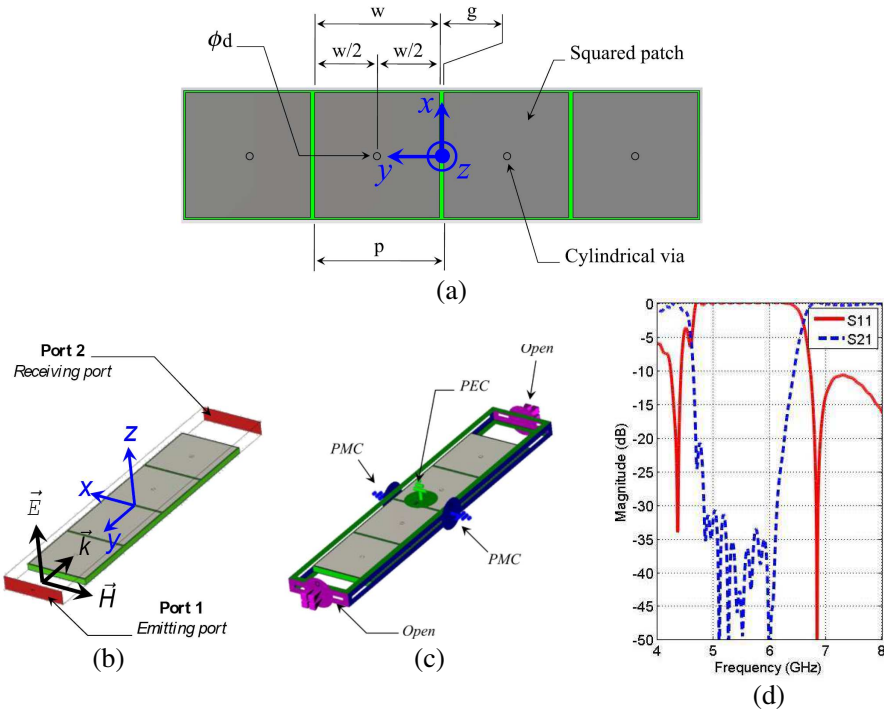

Figure 2. Bandgap computation of the studied EBG matrix, (a) elementary pattern, (b) EBG characterization principle, (c) waveguide boundary conditions and (d) computed reflection (S_{11} (dB)) and transmission (S_{21} (dB)) coefficients.

microwave ports are normally set to the y-axis. The first one (port 1) generates an electromagnetic wave ($\vec{E}$, $\vec{H}$) travelling along the y-axis and received by the port 2.

The boundary conditions (Fig. 2(c)) are chosen in order to define a waveguide structure, for which the four-EBG pattern repeats to infinity along the negative and positive x-direction. This is achieved by setting PMC conditions at both of the x-locations. PEC conditions are moreover defined below and above the substrate, assuming that an infinite ground plane exists onto the rear substrate. Then, two open boundaries are set at the two port locations.

Figure 2(d) depicts the reflection coefficient S_{11} and transmission coefficient S_{21} associated with the computed HIS using the method described in [5, 6] in the 4–8 GHz frequency range. It shows that the bandgap of the MTM matrix (where the entire surface waves are reflected) is included between 4.7 GHz and 6.3 GHz.

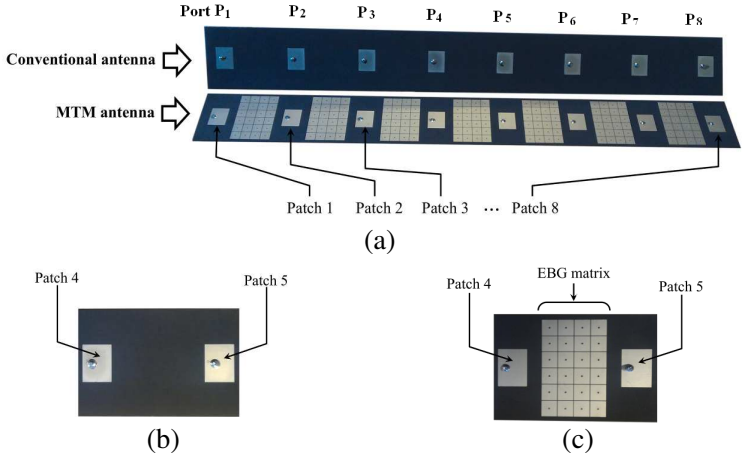

Figure 3. Manufactured antennas, (a) conventional and MTM full antennas, (b) conventional antenna zoom in and, (c) MTM antenna zoom in.

3.2. Antenna Coupling Reduction Using EBG Structures

Two 8-patch antenna arrays (Fig. 3(a)) were designed to run in the MTM bandgap previously pointed out, around 6 GHz. The first antenna is a conventional one, composed of 8 patches of 15.64 mm length and 20 mm width regularly spaced with a 50 mm gap printed on a 503.84 mm $\times$ 67 mm $\times$ 0.787 mm dielectric substrate (RT/Duroid 5880) having a relative permittivity of 2.2 ± 0.02. The second one, hereafter named MTM antenna, consists in the conventional antenna, with 4×6 squared EBG patterns integrated between patches. Detailed structures of these two antennas are presented in Fig. 3(b) and Fig. 3(c) near patches 4 and 5. Specific dimensions of EBG patterns are given Fig. 4.

4. EXPERIMENTAL AND COMPUTED RESULTS

Experimental and computed S-parameters and radiation patterns around 6.0 GHz are compared in this section. Results are presented for patches 2, 4 and 7, located in regions of the antenna where 3 particular mechanical strain states are obtained (Fig. 3(a)). Indeed, close to the twisting system (patch 2) — clamping for the bending tests- maximum mechanical strains will be obtained. On the other hand, close to the bending system (patch 7) — clamping for the twisting tests-mechanical strains are minimal, but important vertical displacement are observed

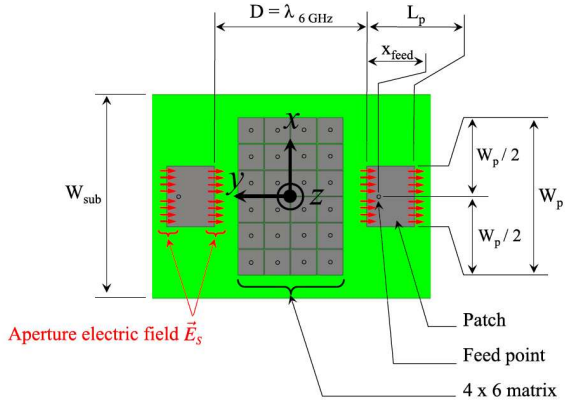

Figure 4. Inserted EBG component ($D = 50\,\text{mm}$, $L_p = 15.64\,\text{mm}$, $W_p = 20\,\text{mm}$, $W_{sub} = 67\,\text{mm}$, $x_{feed} = 4.7\,\text{mm}$).

in bending test. Finally, patch 4 corresponds to an intermediate mechanical behavior.

4.1. *S*-parameters

First, Fig. 5 presents measured (blue) and computed (red) reflective (S_{ii}) and transmitting (S_{ij}, $i \neq j$) parameters in the planar state (non-deformed antenna). The solid and dotted curves respectively correspond to measured parameters for conventional and MTM antennas. Experimental and numerical results are in a good agreement.

It can be observed that the computed reflection parameters S_{ii} have a very good adequacy for both the antennas. On the other hand, a tiny shift (about 20 MHz) can be noted for the experimental ones. The introduction of EBG patterns (MTM antenna) induces a maximal coupling reduction (S_{ij} parameters) about 12 dB through computations and 30 dB through experimental measurements for a 6 GHz frequency. It can also be noted that the experimental bandgap is narrower than the numerical one.

The influence of twisting and bending loads on reflective and transmitting S-parameters, measured with (solid curves) and without (dotted curves) MTM, are respectively shown for a 30° twist angle in Fig. 6 and for a $-70\,\text{mm}$ tip displacement in Fig. 7.

It clearly appears that the S-parameters are non-sensitive to the mechanical distortions, whatever the considered antenna. Moreover, the metamaterial decoupling features are maintained meanwhile the MTM antenna is deformed.

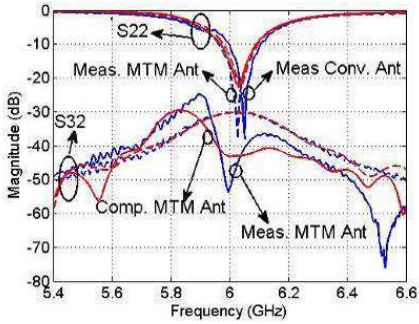

(a) Patch 2

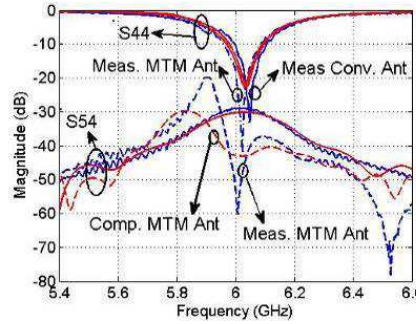

(b) Patch 4

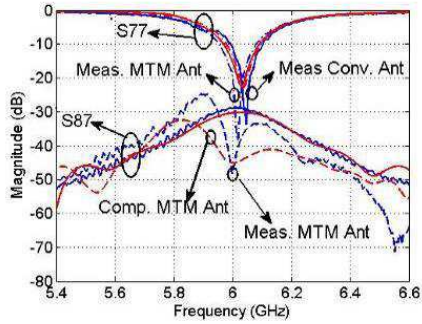

(c) Patch 7

Figure 5. Measured and simulated S-parameters in the planar case.

4.2. Radiation Characteristics

This subsection presents the measured and computed antenna's radiation patterns. The previous mutual coupling parameters (S_{ij}) analysis has shown that the maximal coupling reduction (MTM antenna) is obtained for at 6 GHz. Thus experimental measurements were performed at this frequency.

The radiation pattern has then been measured, on the measurement StarGate (shown by Fig. 8) of the SATIMO Industries. It consists in an arch, installed in a $5 \times 5 \times 5\,\mathrm{m}^3$ anechoic chamber. The antenna under test (AUT) mounted on the deformation device is located on the top of a mast such as to be at the center of the arch. The arch is equipped with several probes, regularly spaced around the perimeter, being able to work in emitting or receiving mode. Concerning our test measurement, the probes are set in receiving mode, in order to acquire the radiation patterns along the θ elevation angle,

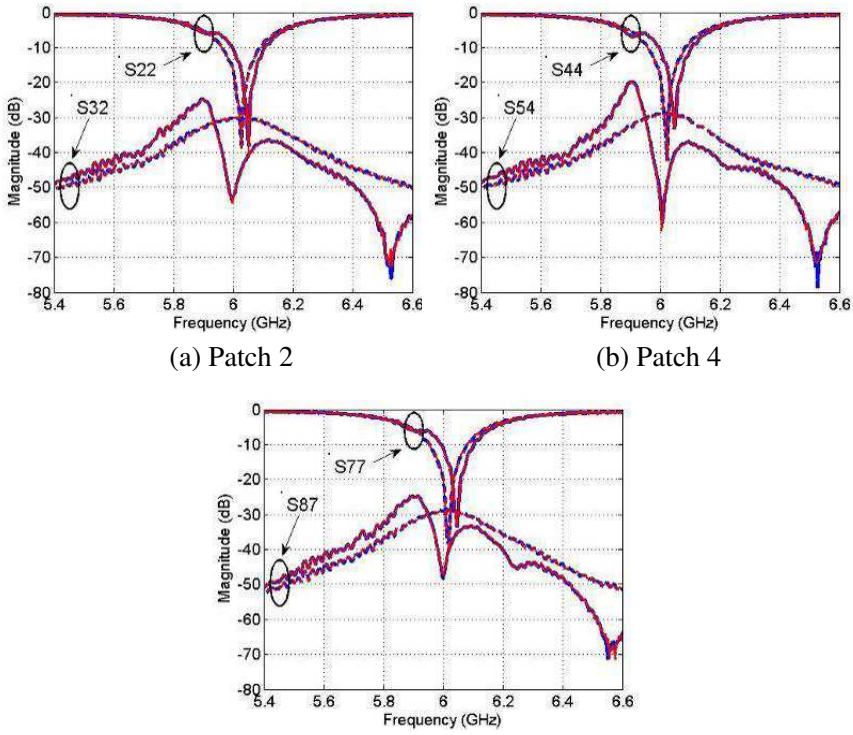

(a) Patch 2 (b) Patch 4

(c) Patch 7

Figure 6. Measured S-parameters in the planar (blue) and twisted (red) configurations.

corresponding to each ϕ azimuth angle reached through the rotation of the mast.

Figure 9 illustrates the bended and twisted configurations of the AUT, and assembling of the antenna on the support (Fig. 9(b)).

Each of the eight patches of the array antenna was characterized and separately fed while all the others were $50\,\Omega$ adapted such as to avoid radiation interferences. The reflector plane is finite size metallic ground plane (or perfect electric plane, PEC).

4.2.1. Planar Configuration

Figure 10 presents the measured and computed E-plane (Fig. 10(a)) and H-plane (Fig. 10(b)) Cartesian radiation diagrams obtained for patch 4, located in the middle of the patch network, in the planar case (non-deformed structure), for the conventional and MTM antennas.

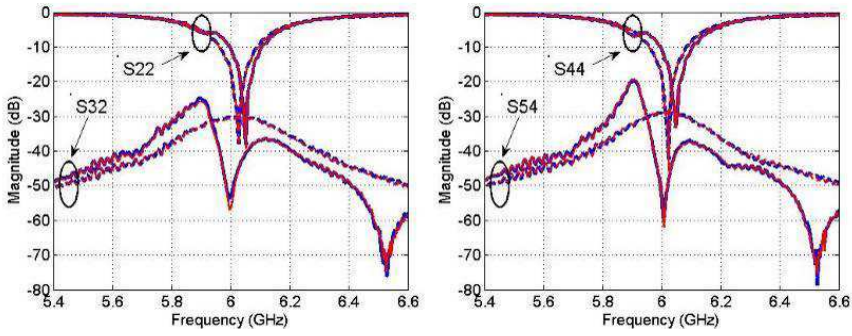

(a) Patch 2 (b) Patch 4

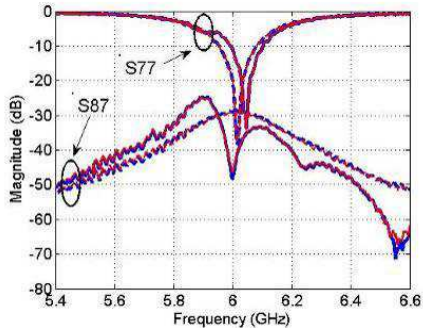

(c) Patch 7

Figure 7. Measured S-parameters in the planar (blue) and bended (red) configurations.

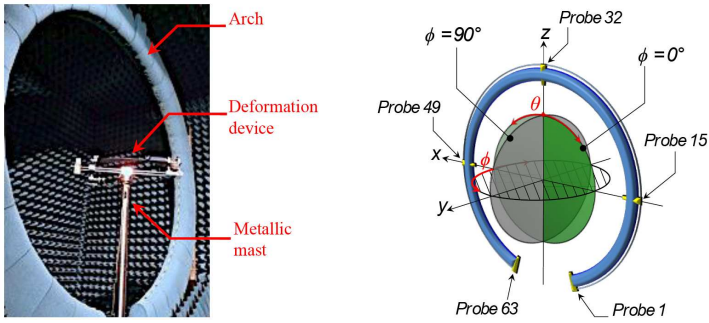

Figure 8. The measurement StarGate of the SATIMO industries.

It appears that the computed results are in good agreement with the measured radiation pattern in the $[-60°, 60°]$ elevation angle range (θ), but "edges effects" can be observed out of this range.

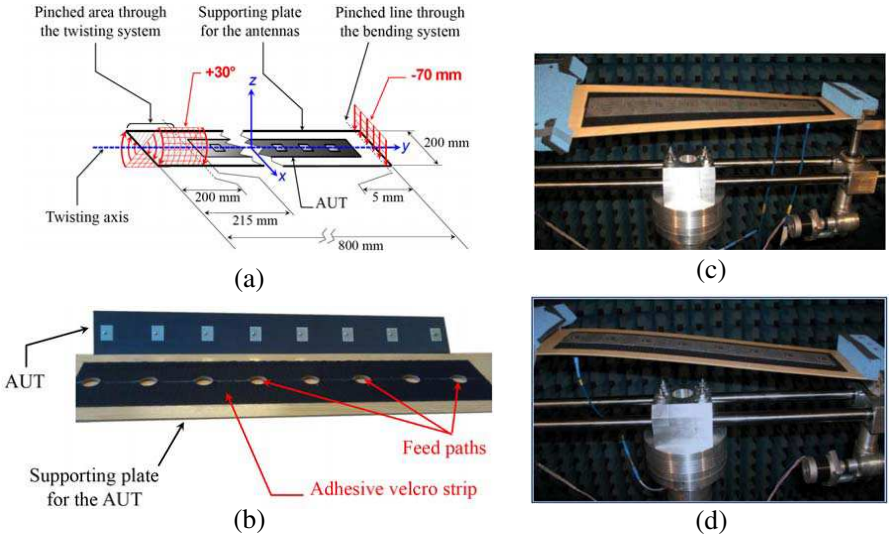

Figure 9. The AUT and its supporting plate, (a) mechanical boundary conditions, (b) components of the assembly, (c) +30° Twisted AUT et (d) −70 mm bended AUT.

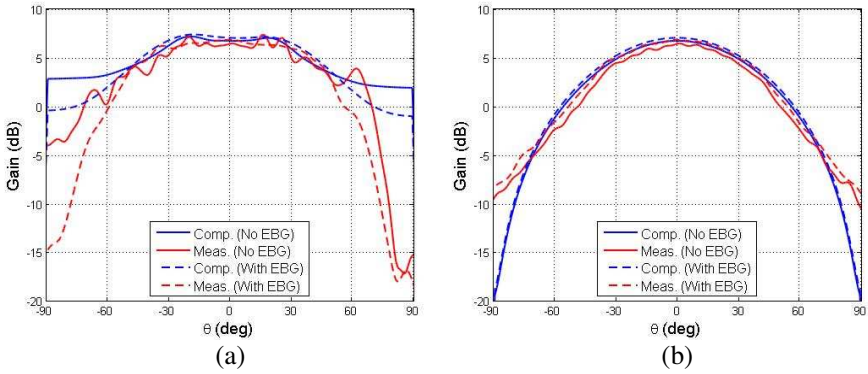

Figure 10. Cartesian radiation diagrams of patch 4, in (a) *E*-plane and (b) *H*-plane.

This point could be explained as follows: the measured antennas were manufactured with a finite metallic ground plane, and consequently, the radiation characteristics are available in the whole free space, i.e., the angular range goes from −180° to 180°. On the other hand, as the patch antenna model corresponds to a cavity recessed in an infinite metallic ground plane model, the radiation

patterns computed with CST software were post-processed in the upper half-space, i.e., an angular range from $-90°$ to $90°$ in the elevation view. Then, the contribution of lower half-space electromagnetic fields can not be taken into account via this numerical model.

Finally, it can be noticed in Fig. 10 that the main lobe (ML) directions are respectively 0-degree (vertical) in the H-plane and ± 18-degrees oriented from the vertical axis in the E-plane diagrams, for conventional and MTM antennas. The EBG structures do not affect the radiation patterns. Moreover, it reduces the back radiation especially in the E-plane.

Figure 11 presents the total gain of the conventional and MTM antennas in the planar configuration. It is obtained by summing the individual gain of each of the 8 patches.

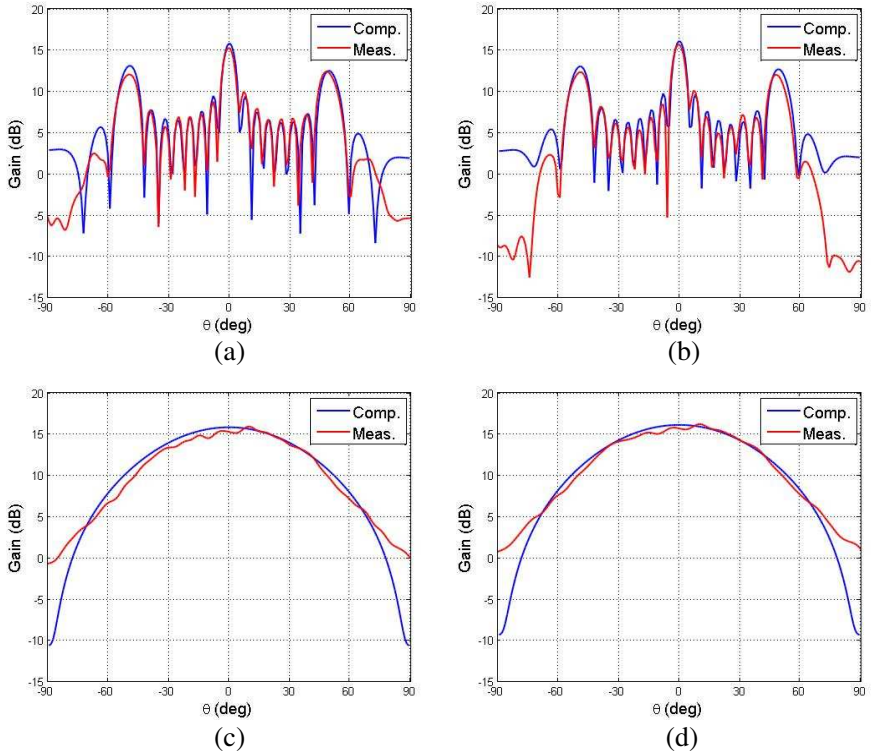

Figure 11. 8 patches Cartesian radiation diagrams, (a) E-plane for the conventional antenna, (b) E-plane for the MTM antenna, (c) H-plane for the conventional antenna, (d) H-plane for the MTM antenna.

It can be noticed that the measured data are well estimated by CST EM numerical model. Moreover, the unitary radiation patterns combination leads to a main lobe and some side secondary lobes, due to the patch interspaces corresponding to $D_{patches} = \lambda_{6\,\mathrm{GHz}}$.

4.2.2. Twisting Effects

Figure 12 presents the impact of a 30-degrees twisting angle on measured H-plane polar radiation patterns for patch 2, located close to the maximal mechanical strains zone (close to the twisting systems) for the conventional (red curves) and MTM (blue curves) antennas.

It can be observed that the impact of the twisting (dotted curves) lies in a tilt about 28 degrees of the H-plane radiation diagram in comparison with the planar configuration (solid curves), whatever the considered antenna. On the other hand, the shapes of polar radiation diagram seem to be non-sensitive to this mechanical distortion whatever the considered antenna. Finally, the EBG structures do not affect the radiation patterns.

4.2.3. Bending Loads

Figure 13 presents the impact of a 70 mm tip bending displacement load on measured E-plane polar radiation patterns for patch 4, located in the middle of the patch network, close to the maximal mechanical strains, for the conventional (red curves) and MTM (blue curves) antennas. It can be observed that the impact of the bending (dotted

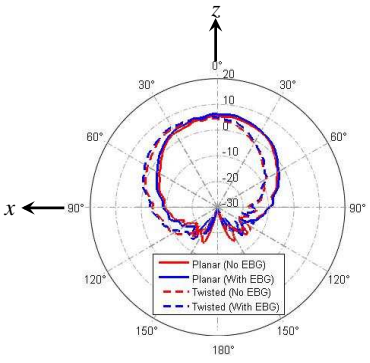

Figure 12. Impact of twisting on the H-plane polar patterns for the patch 2.

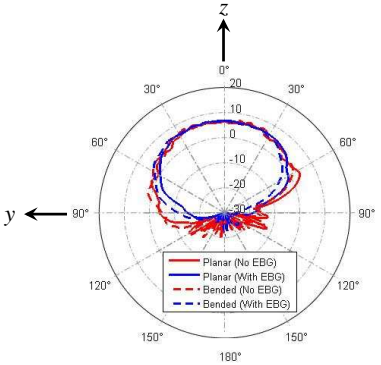

Figure 13. Impact of bending on the E-plane polar patterns for patch 4.

curves) lies in a tilt about 11 degrees of the E-plane radiation diagram in comparison with the planar configuration (solid curves), whatever the considered antenna. Moreover, contrary to the twisting case, the implementation of EBG structure induces a slight modification in the radiation pattern shapes in planar and deformed configurations.

Finally, the impacts of twisting and bending distortions on the total radiation patterns are presented in Fig. 14 (Cartesian) and Fig. 15 (3D). The patterns are plotted in the cut planes in which the deformation influence is logically expected. Accordingly, the twisting effects are observed in the H-plane, while bending ones are observed in the E-plane. It can be observed that the Main Lobes respectively shift about $-13°$ and $-8°$ for the twisting and bending distortion compared to the non-deformed configuration.

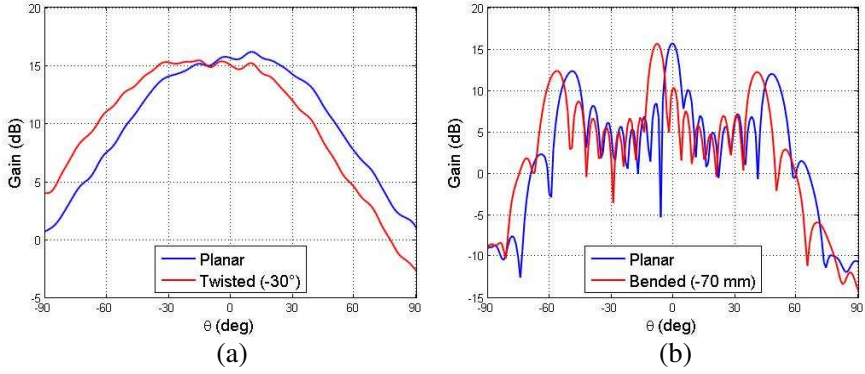

Figure 14. Combined Cartesian pattern, (a) "Planar-Twisted" measurement — H-plane, and (b) "Planar-Bended" measurement — E-plane.

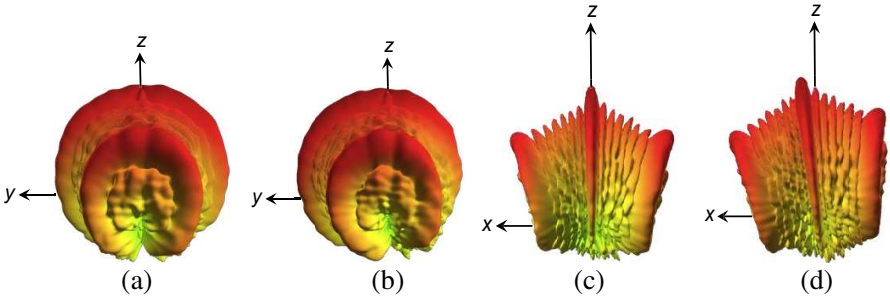

Figure 15. Recombined 3D polar pattern, (a) planar, y-z view, (b) twisted, y-z view, (c) planar, x-z view and (d) bended, x-z view.

5. CONCLUSIONS

The influence of the prescribed mechanical deformations to an EBG metamaterial-based antenna is investigated in this paper. Two antennas have been manufactured: the first one is a conventional antenna, composed of eight rectangular patches, whereas the other one is equipped with squared EBG metamaterial structures, located between the seven couples of patches. The EBG structures are used here to reduce the mutual coupling. A 30 dB reduction has been achieved according to some measurements performed around the resonant frequency.

A mechanical experimental setup has been conceived to study the electromagnetic behavior of the twisted and bended antennas. Results show that the metamaterial performances of the EBG-based antenna are not modified. Nevertheless, it is only observed that the main lobe direction is sensitive to the structural deformation of the antenna.

In future works, it would be interesting to study other designs of EBG-based patch antennas, so as to answer whether these conclusions could be generalized.

ACKNOWLEDGMENT

The authors would like to thank INEO Defense for having manufactured the antennas, and also thank SATIMO Industries for the use of their measurement facilities.

REFERENCES

1. Yang, F. and Y. Rahmat-Samii, *Electromagnetic Bandgap Structures in Antenna Engineering*, The Cambridge RF and Microwave Engineering Series, 2009.
2. Sievenpiper, D., "High impedance electromagnetic surfaces with a forbidden frequency band," *IEEE Transactions on Microwave Theory and Techniques*, Vol. 47, No. 11, 2059–2074, 1999.
3. Han, X., H. Hafdallah Ouslimani, and A. C. Priou, "Understanding the coupling reduction effect in microtrip array antennas using high impedance surface (HIS)," *APS-S/URSI 2011*, Spokane, Washington, Jul. 3–8, 2011.
4. Kawakami, Y. and T. Hori, "Mutual coupling reduction effects of EBG structure located on cylinder surface," *2010 IEEE Antennas and Propagation Society International Symposium (APSURSI)*, 1–4, 2010.

5. Liang, L., C. H. Liang, L. Chen, and X. Chen, "A novel broadband EBG using cascaded mushroom-like structure," *Microwave and Optical Technology Letters*, Vol. 50, No. 8, 2167–2170, 2008.
6. Tran, C. M., H. Hafdallah-Ouslimani, L. Zhou, A. C. Priou, H. Teillet, J.-Y. Daden, and A. Ourir, "High impedance surfaces based antennas for high data rate communications at 40 GHz," *Progress In Electromagnetic Research C*, Vol. 13, 217–229, 2011.
7. Han, X., H. Hafdallah-Ouslimani, T. Zhang, and A. C. Priou, "CSRRS for efficient reduction of the electromagnetic interferences and mutual coupling in microstrip circuits," *Progress In Electromagnetics Research B*, Vol. 42, 291–309, 2012.
8. Schurig, D., J. J. Mock, and D. R. Smith, "Electric-field-coupled resonators for negative permittivity metamaterials," *Applied Physics Letters*, Vol. 88, No. 4, 41109–41109-3, 2006.
9. Hafdallah Ouslimani, H., X. Han, and T. Zhang, "Analysis and reduction of electromagnetic coupling interferences in microstrip antenna arrays," *Advanced Electromagnetics Symposium AES 2012 Special Issue, META12*, Paris, 2012.
10. Adnet, N., "Modélisation numérique du couplage mécanique/électromagnétique pour l'étude de la sensibilité du comportement électromagnétique d'antennes patch aux déformations mécaniques," Ph.D. Thesis, University Paris, Ouest, 2012.
11. http://www.cst.com/content/products/mws/overview.aspx.